Journal of Physiology (1993), **462**, *pp.* 393–420
With 12 figures
Printed in Great Britain

HYPERPOLARIZATION-ACTIVATED CURRENTS IN ISOLATED SUPERIOR COLLICULUS-PROJECTING NEURONS FROM RAT VISUAL CORTEX

BY JOEL S. SOLOMON AND JEANNE M. NERBONNE

From the Department of Molecular Biology and Pharmacology, Washington University School of Medicine, St Louis, MO 63110, USA

(*Received 20 January 1992*)

SUMMARY

1. *In vivo* injections of rhodamine beads into the superior colliculus of 4–9 postnatal day rat pups label a population of layer 5 cells in the primary visual cortex that can be identified in tissue sections or dissociated cell cultures.

2. Under voltage clamp, hyperpolarizations of isolated superior colliculus-projecting (SCP) neurons from rest elicit an instantaneous inward current (I_{inst}) with nearly linear current–voltage properties that is not blocked by extracellular application of 3 mM CsCl.

3. Voltage clamp steps to potentials more negative than −60 mV evoke a slowly activating, non-inactivating inward current that is not blocked by 1 μM TTX, 1 mM 4-aminopyridine (4-AP), 5 mM Co^{2+}, or 25 mM TEA, but is potently blocked by extracellular application of 3 mM CsCl. This current is similar to I_h described in other systems.

4. I_h, the time-dependent inward current in SCP neurons, begins to activate near the resting membrane potential and reaches full activation at −110 mV. The voltage dependence of activation is well fitted by a Boltzmann distribution with the membrane potential at half-maximal activation ($V_{\frac{1}{2}}$) = −81·0 mV and s (steepness of the curve parameter) = 7·2 mV. Thus, I_h may contribute to setting the resting membrane potential and resting input resistance of SCP neurons.

5. The inward rectification of the whole-cell current *vs.* voltage relation is accounted for by the voltage dependence of I_h activation. Current through the activated h-conductance shows slight outward rectification that is accounted for by constant field considerations.

6. The h-conductance is substantially permeable only to sodium and potassium and, under normal physiological conditions, is expected to reverse at approximately −22 mV at 20 °C. For $[K^+]_o \leqslant 20$ mM and $120 \text{ mM} \geqslant [Na^+]_o \geqslant 70$ mM, I_h obeys independence with a P_{Na}/P_K (ratio of Na^+ to K^+ permeability) of 0·40.

7. Extracellular potassium increases g_h. If this effect is modelled as the result of potassium binding to an extracellular conductance-permitting site, potassium has an apparent dissociation constant (K_{app}) of 25·7 mM and the ability to maximally increase g_h in the order of 10-fold over basal levels.

8. I_h underlies the depolarizing 'sag' and 'overshoot' observed in SCP neurons

following the onset and offset, respectively, of hyperpolarizing current injections. In addition, I_h appears to control the duration and the frequency of repetitive firing following the cessation of sustained hyperpolarizing current injections. Taken together, these results suggest that I_h plays an important role in modulating the response of SCP neurons to inhibitory and excitatory synaptic inputs.

INTRODUCTION

Although much is known about information processing and synaptic interconnectivity in the cerebral cortex, the details of the electrical signal transformations performed by individual cortical neurons are not well understood. This appears to result primarily from the extraordinary diversity of cell types in the cortex and the difficulties associated with reliably identifying and studying the properties of different cell types. *In vitro* microelectrode recordings in cortical slices suggest that the intrinsic membrane properties of different cortical neurons vary substantially (for review, see Connors & Gutnick, 1990). For example, even within cortical layer 5, a layer known to be composed primarily of large pyramidal cells, intracellular recordings have revealed that different pyramidal cells display distinct types of activity patterns in response to depolarizing current injections. Both 'regular spiking' and 'burst firing' cells have been distinguished (Connors & Gutnick, 1990; Mason & Larkman, 1990).

Because laminar location is not a sufficient criterion to distinguish different cortical neuronal types, we have chosen to use *in vivo* retrograde labelling techniques to identify, based on their projection targets, a subpopulation of layer 5 visual cortical neurons for further study in dissociated cell culture. By combining retrograde labelling with patch clamp recording of isolated cells in culture, we are investigating the intrinsic membrane properties of a subpopulation of visual cortical projection neurons in detail. Because we retain the anatomical information about the cells by prior labelling, we anticipate that it will be possible to reintegrate our results into the body of information derived from intact systems. This strategy for identifying cortical cell types has recently proved useful in investigations of both ligand-gated (Huettner & Baughman, 1986) and voltage-activated (Giffin, Solomon, Burkhalter & Nerbonne, 1991) conductances. Furthermore, the study of identified cortical neurons in dissociated cell culture permits precise control of the extracellular and intracellular environments and reliable spatial control of the membrane voltage under voltage clamp.

The work described here employs two variations of the whole-cell patch clamp technique, conventional whole-cell recording (Hamill, Marty, Neher, Sakmann & Sigworth, 1981) and nystatin perforated patch recording (Horn & Marty, 1988), to examine hyperpolarization-activated conductances in layer 5 cells of rat visual cortex that project to the superior colliculus (SCP cells). Recordings in slices of rat visual cortex have previously demonstrated that the response of visual cortical neurons to cell hyperpolarization is heterogeneous across cortical layers and even within layer 5 (Mason & Larkman, 1990). We have chosen SCP neurons in rat primary visual cortex as an anatomically and morphologically homogeneous cortical cell *type* (Schofield, Hallman & Lin, 1987; Hallman, Schofield & Lin, 1988) in

which to characterize the conductances underlying the cellular response to hyperpolarization.

METHODS

Identification of projection neurons

SCP neurons from area 17 were identified *in vitro* following *in vivo* retrograde labelling with rhodamine-conjugated latex 'beads' using methods similar to those previously described (Katz, Burkhalter & Dreher, 1984; Thong & Dreher, 1986). Briefly, 4–6 postnatal day (4–6 PD) Long Evans rat pups were anaesthetized with 1% halothane in air and secured in a plaster mould within a stereotaxic frame. Following craniotomy, a glass micropipette was guided to the area of the left superior colliculus and nanolitre quantities of beads were pressure injected in 1–3 sites. The scalp was sutured closed and the animal permitted to recover from anaesthesia before being returned to its mother. After allowing at least 24 h for retrograde transport of the beads, animals were killed either by transcardial perfusion with fixative or cervical dislocation (see below). Bead-containing SCP neurons were identified in slide-mounted microtome sections or dissociated cell culture of the ipsilateral area 17 under epifluorescence optics (see below). The injection sites were verified by direct inspection.

For identification of bead-containing SCP neurons in coronal sections through area 17, pups were anaesthetized by intraperitoneal injection of sodium pentobarbitone (80 mg/kg) and killed by transcardial perfusion with 4% paraformaldehyde in 0·1 M phosphate buffer at 0 °C. The brains were removed and stored overnight at 4 °C in a 4% paraformaldehyde solution containing 30% sucrose. Coronal sections, 50 μm thick, cut on a freezing microtome, were then mounted on gelatin-coated glass slides, briefly dehydrated and cleared in ethanol and xylene, respectively, and covered with Krystalon. Alternate sections were stained with Cresyl Violet (Nissl stain) to reveal the cortical laminae and the cytoarchitectonic boundaries of area 17.

The morphology of SCP neurons *in situ* was examined in coronal sections of visual cortex stained with the fluorescent tracer DiI (1,1′-dioctadecyl-3,3,3′,3′-tetramethylindocarbocyanine perchlorate). In these experiments, pups were anaesthetized and perfused as described above. Following at least 24 h post-fixation in 0·1 M phosphate buffer containing 4% paraformaldehyde and 30% sucrose, a small crystal of DiI was placed within a superficial incision made in the superior colliculus. Brains were then immersed in a 1% paraformaldehyde solution and stored in a light-proof container at 30 °C for at least 6 months. At various incubation times, brains were cut on a vibratome, and 100 μm thick coronal sections of occipital cortex were examined under epifluorescence illumination (see Fig. 1). Although we have not examined the time course of DiI labelling quantitatively, the extent of labelling does vary as a function of the incubation time. In particular, longer incubation times markedly improved the extent of dendritic labelling.

Dissociation and cell culture

For the preparation of dissociated cortical cultures, animals were killed by rapid cervical dislocation and the brains were rapidly removed. Cortical astrocyte, 'feeder layer' cultures were prepared from 6 PD Long Evans rat pups according to published procedures (Raff, Fields, Hakomori, Mirsky, Pruss & Winter, 1979). Following isolation, cells were suspended in Minimum Essential Medium (MEM) containing 25 mM KCl, 100 units ml^{-1} penicillin/streptomycin, and 10% heat-inactivated fetal calf serum, and plated at a density of $2–3 \times 10^5$ cells cm^{-2} on poly-L-lysine-coated glass coverslips attached to the bottoms of modified tissue culture dishes. Cultures were maintained at 37 °C in a humidified atmosphere of 95% air–5% CO_2, and fresh culture medium was added every 2 days. After the cells reached confluence, 10^{-5} M cytosine arabinoside was added to the medium for 24 h to eliminate fibroblasts and other rapidly dividing cells. Cultures prepared in this manner contain $\geqslant 95\%$ astrocytes, identified by glial fibrillary acidic protein immunoreactivity, and are useful substrates for culture of cortical neurons for at least 4 weeks (J. P. Doyle & J. M. Nerbonne, unpublished observations).

Cortical neurons were dissociated from 5–15 PD Long Evans rat pups following bead injections at 4–6 PD using a modification of the procedure of Huettner & Baughman (1986), as described previously (Giffin *et al.* 1991). Cells were suspended in MEM supplemented with 500 μM glutamine, 100 units/ml^{-1} penicillin/streptomycin, and 10% heat-inactivated horse serum, and plated on astrocyte 'feeder layer' cultures at a density of $\sim 1·5 \times 10^5$ cells/ml. Cultures were maintained in

a 95% air–5% CO_2 incubator at 37 °C. Cortical neurons can be maintained in culture for at least 2 weeks.

Electrophysiological recording

Electrophysiological experiments were performed on SCP neurons within the first 48 h after isolation using the whole-cell variation of the patch clamp technique (Hamill *et al.* 1981) or the nystatin perforated patch technique (Horn & Marty, 1988). Recordings were obtained at room temperature (20–22 °C) using a Dagan Model 8900 patch clamp amplifier with a 1 GΩ feedback resistor (Dagan, USA). Current records were low-pass filtered on line at 2 kHz with an 8 pole Bessel filter (Frequency Devices, USA). Experimental protocols were controlled and data were collected using pCLAMP software (Axon Instruments, USA) on an IBM-AT computer equipped with a Tecmar Labmaster (TL-1) interface to the electrophysiological equipment. For experiments designed to examine the effects of I_h activation on the firing properties of SCP neurons, the clamp was modified to allow rapid switching between the voltage clamp and current clamp modes. This was accomplished by replacing the operating switch of the amplifier with two transistor–transistor logic (TTL)-activated double pole, single throw reed relays (Magnetcraft 118-DIP1). The timing of the TTL pulses was controlled through the TL-1 interface using pCLAMP. Whole-cell recording pipettes were drawn on a two-stage puller from soda lime glass capillary tubes (Kimble 73811). Tip diameters were typically 1 μm. Pipette shanks were coated with Sylgard to within 5–10 μm of the tip to reduce pipette capacitance. Pipettes were then fire-polished over a glass-coated platinum filament (Narashige, Japan), and stored in a closed container until use.

SCP cells, identified under epifluorescence illumination, were visualized under phase contrast illumination on an inverted microscope (Nikon, USA) at 400×. All seals were $\geqslant 8$ GΩ. Pipette series resistances, determined from the series resistance compensation potentiometer on the amplifier, were always $\leqslant 5$ MΩ and were stable throughout the recordings. This probably represents a maximum uncompensated series resistance of ≈ 7 MΩ (see below).

Nystatin perforated patch recording pipettes were drawn from borosilicate glass capillary tubes (Boralex) and prepared for recording as described above for whole-cell recording. At the time of recording, the pipette was filled by submerging the tip in nystatin-free solution while applying suction to the back of the pipette using a 1 ml syringe. The pipette was then back-filled with a sonicated nystatin-containing pipette solution (see Table 1) that was prepared from a 50× stock solution in dimethylsulphoxide immediately before recording. Following formation of a gigaseal, all suction was removed from the pipette. Electrical access to the cell interior was achieved over the following 1–30 min as the pore-forming antibiotic permeabilized the membrane patch. Latency of permeabilization of the membrane patch was the most variable parameter in achieving stable recordings and was very sensitive to the amount of nystatin-free solution present in the pipette tip. The progress of membrane permeabilization was reflected by the gradual increase in the height and rate of decay of the capacitance transient following periodic 10 mV hyperpolarizing test pulses. Series resistance (R_{ser}) stabilized in 10–45 min and its magnitude was determined by division of the capacitance current decay time constant (τ_{clamp}) by the cell membrane capacitance (C_{mem}). Under recording conditions in which the seal resistance is very high and the capacitance of the pipette has been compensated, the time course of the capacitance transient decay in a cell that is modelled as a parallel resistor and capacitor, is a single exponential process whose time constant is approximated by the expression:

$$\tau_{clamp} \approx \left(\frac{R_{in}R_{ser}}{R_{in}+R_{ser}}\right)C_{mem}, \tag{1}$$

where R_{in} is the cell membrane resistance. C_{mem} was calculated by integration of capacitance transients during ±10 mV steps from a holding potential of −60 mV. τ_{clamp} was determined by fitting of the capacitance transient decay to an equation of the form:

$$I = A_0 + A_1 e^{-\frac{t}{\tau}}, \tag{2}$$

where I is the current amplitude, A_0 and A_1 are free parameters, and t is time from the peak of the capacitance spike. Because R_{ser} is very small with respect to R_{in}, eqn (1) reduces to

$$\tau_{clamp} = R_{ser}C_{mem}.$$

Division of τ_{clamp} by C_{mem}, therefore, yields an estimate of R_{ser}. The total series resistance for

nystatin recordings was (mean ± S.D.) 34·0 ± 4·6 MΩ and was compensated 42 ± 12 %. The maximum voltage error (which is uncompensated R_{ser} I_{max}), therefore, was ⩽ 4·5 mV.

The compositions of the recording solutions are given in Table 1. In voltage clamp experiments, tetrodotoxin (TTX) was used to block voltage-activated sodium channels; tetraethylammonium (TEA) and 4-aminopyridine (4-AP) were used to suppress depolarization-activated outward

TABLE 1. Recording solutions[a]

Solution	[Na^+]	[K^+]	[Cl^-]	[Mg^{2+}]	[Ca^{2+}]	[EGTA]	[Co^{2+}]
Pipette[b]							
K_{pip}	1·5	140	140	3	—	10	—
K-Ca_{buf}	1·5	140	144·1	3	2·07	10	—
Nystatin	—	195	69	7	—	—	—
Bath[d]							
Normal	140	4	153	2	2·5	—	—
Block	120	4	153	2	0·5	—	2
ΔK[e]	70	0, 0·5, 1, 5, 20, 50	105, 105·5, 106, 110, 125, 155	2	0·5	—	5
ΔNa[e]	3, 10, 100, 120	5	43, 50, 140, 160	2	0·5	—	5
ΔNaΔK[e]	0, 10, 30, 50, 100	70, 60, 40, 20, 20	105, 105, 105, 105, 155	2	0·5	—	5
ΔCl[f]	10	5	150	2	0·5	—	5

All concentrations in millimolar.

[a], all solutions contained 5 mM glucose and 10 mM *N*-2-hydroxyethylpiperazine-*N'*-2-ethanesulphonic acid (Hepes) adjusted to pH 7·3 with KOH, NaOH, or TRIS base.

[b], all whole-cell pipette solutions also contained 3 mM ATP and 0·5 mM GTP.

[c], nystatin pipette solution also contained 70 mM SO_4^{2-}, 0·1 mg/ml nystatin, and 0·2 % DMSO.

[d], bath solutions contained 1 μM TTX, 20 mM TEA, and 1 mM 4-AP except as noted in the text.

[e], sucrose was added to bring solution osmolarity to 310 mosM.

[f], 100 mM choline chloride was added to bring solution osmolarity to 310 mosM.

potassium currents. These compounds, at the concentrations used, did not alter I_h. Voltage-activated calcium currents were also blocked in many experiments by the addition of $CoCl_2$. In some experiments, intracellular calcium was buffered to 100 nM with pipette solution containing ethylene glycol-bis-(aminoethylether)-*N,N,N',N'*-tetraacetic acid (EGTA). The appropriate proportions of $CaCl_2$ and EGTA were determined by titration of 10 mM EGTA at pH 7·3 and in the presence of 3 mM $MgCl_2$ using a Ca^{2+}-sensitive electrode. In the permeability studies, osmotic balance was maintained following manipulations of extracellular Na^+ and K^+ by the addition of sucrose.

During whole-cell recordings, experimental solutions were applied to the cell exterior by pressure ejection from glass pipettes similar to those used for electrical recordings. The pipette tips were typically 2–4 μm in diameter and were placed 5–15 μm from the cell surface.

Data analysis

Analysis of digitized data was performed using pCLAMP analysis programs, Excel (Microsoft Corporation, USA), CSS:Statistica (StatSoft, USA), and NFIT (Island Products, USA). All summarized data are expressed as means ± S.D. unless indicated otherwise. Statistical significance was set at the $P < 0·05$ level.

The adequacy of spatial control of the membrane voltage was determined by exponential fitting of the decays of the capacitance transients recorded during ± 10 mV steps from a holding potential of −60 mV according to eqn (2). Cells with decays that were well fitted by single exponentials, i.e. the contributions of secondary exponential components represented < 3 % of the amplitude of the primary exponential, were considered to behave as a single electrical compartment. The 3 % criterion was established because our analyses revealed that when the second exponential was ⩽ 3 % of the amplitude of the first component, the data were equally well-described by a single

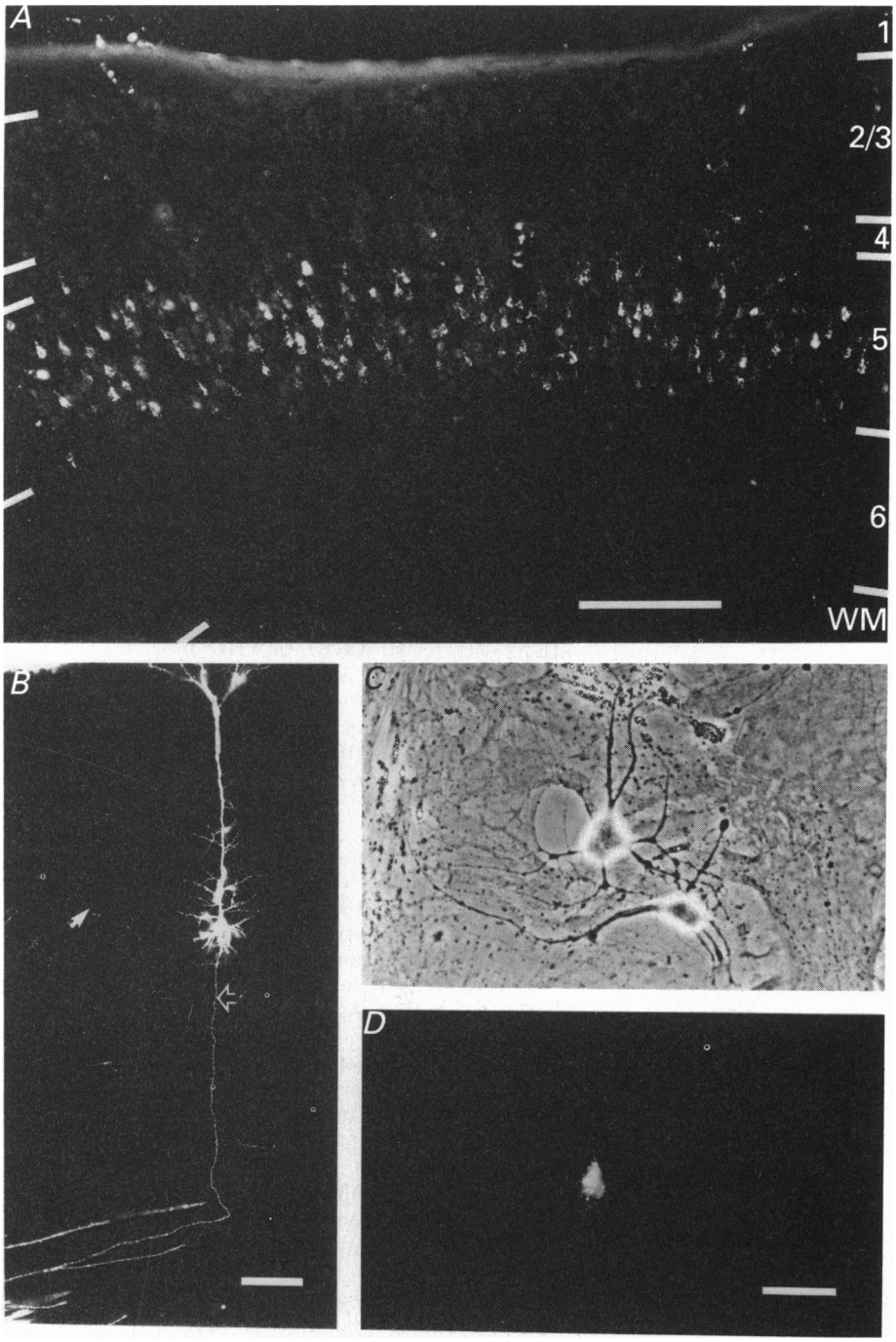

Fig. 1. Identification of area 17 superior colliculus-projecting (SCP) neurons in tissue sections and dissociated cell cultures. *A*, bead-labelled SCP neurons in a 50 μm coronal section of primary visual cortex of a postnatal day 13 rat were photographed under rhodamine epifluorescence optics. Boundaries of cortical laminae were determined from an adjacent Nissl-stained section. SCP cell bodies are localized to cortical layer 5. Scale bar, 150 μm. *B*, photomontage of a SCP neuron. DiI staining in this 100 μm coronal

exponential. Although, on visual inspection, there were no obvious morphological differences between the cells that satisfied this criterion and those that did not, it is reasonable to assume that cells not well described by single exponentials had elaborated more fine processes *in vitro*. Only data obtained from cells satisfying the criterion above were analysed further.

Materials

Pregnant Long-Evans rats were obtained from Harlan Sprague Dawley. MEM was obtained from Gibco. Fetal bovine serum was obtained from C.C. Supplies (Cleveland, OH, USA) and horse serum from Hyclone (Logan, UT, USA). Papain was purchased from Worthington (Freehold, NJ, USA). Sylgard is a product of Dow-Corning. Krystalon (EM Diagnostic Systems (Gibbstown, NJ, USA)), DiI (Molecular Probes, Inc., Eugene, OR, USA), and rhodamine beads (Lumafluor (New City, N.Y., USA)) were generously donated by Dr Andreas Burkhalter, Washington University Medical School, Department of Neurosurgery. All other chemicals were purchased from Sigma Chemical Co. Kimble glass capillary tubes were obtained from VWR Scientific (Chicago, IL, USA), and Boralex capillaries were obtained from Rochester Scientific (Rochester, NY, USA).

RESULTS

Identification of SCP neurons

The injection of rhodamine-conjugated latex microspheres or 'beads' into the left superior colliculus of 4–6 PD rat pups retrogradely labels the cell bodies and proximal dendrites of superior colliculus-projecting (SCP) neurons in primary visual cortex (Fig. 1*A*). Consistent with previous reports (Thong & Dreher, 1986; Schofield *et al.* 1987), SCP cells are uniformly large pyramidal neurons whose cell bodies are restricted to cortical layer 5. DiI staining of fixed tissue reveals that SCP neurons are long pyramids (Schofield *et al.* 1987) possessing basal dendrites that extend into layers 5 and 6, and a large apical trunk (Larkman & Mason, 1990) that extends up to layer 1 where it ends in characteristic tuft (Fig. 1*B*). Following *in vivo* retrograde labelling with beads, SCP neurons can be identified in dissociated cell culture (Huettner & Baughman, 1986; Giffin *et al.* 1991) using epifluorescence optics. Bead-containing cells can be easily distinguished from unlabelled area 17 neurons (Fig. 1*C* and *D*). They make up 0·1–1·0% of the neurons in cultures of area 17, and are amongst the largest neurons present. The means (±S.D.) input resistance in normal bath solution (Table 1) of SCP neurons examined 12–30 h after isolation was 954±450 MΩ ($n = 12$). The whole-cell capacitance of these cells was typically 20–30 pF. The means (±S.D.) resting membrane potential, measured using the perforated patch recording technique, was −66±6 mV ($n = 6$). Although bead-labelled cells may have pyramidal cell bodies, a large 'apical' trunk and extensive dendrites at the time of dissociation, these processes retract over the first few hours in culture. The rate and quality of process re-extension in culture is highly variable,

section of postnatal day 8 rat visual cortex illustrates the large pyramidal cell body, thick, tapering apical dendrite, and terminal tuft characteristic of area 17 SCP neurons. After placement of the DiI crystal in the superior colliculus, this sample was stored in fixative for 11 months prior to sectioning. Numerous basal dendrites extend from the cell body, as well as a single axon (open arrow) that gives rise to intracortical collaterals (closed arrow) before entering the subcortical white matter. Scale bar, 50 μm. *C*, phase contrast photomicrograph of primary visual cortical neurons dissociated on postnatal day 13 and maintained 2 days *in vitro* on a monolayer of cortical astrocytes. *D*, rhodamine epifluorescence micrograph of the same field as in *C*. Note that, of the two neurons shown in *C*, only one contains beads in its cell body and neurites, indicating that *in vivo*, this cell projected an axon to the superior colliculus. Scale bar in *C*, 25 μm and applies also to *D*.

making cell morphology *in vitro* an unreliable indicator of neuronal type. Contrastingly, rhodamine beads are retained in the cells and, therefore, remain a dependable identifier of SCP neurons even in long-term cultures (see also Huettner & Baughman, 1986).

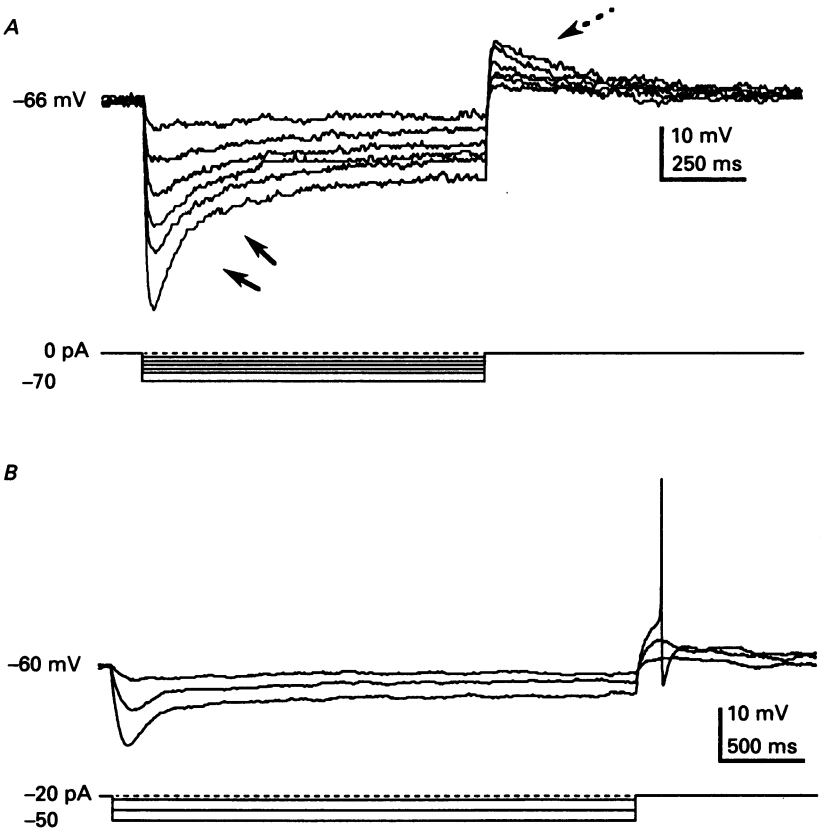

Fig. 2. Sag and overshoot phenomena in response to hyperpolarizing current injections. *A*, whole-cell current clamp recording in normal bath solution (Table 1) containing 1 μM TTX. Small, sustained current injections result in low amplitude hyperpolarizations that are maintained for the duration of the test pulse. On larger hyperpolarizing current injections, the membrane potential *sags* (solid arrows); the magnitude and the rate of the sag increase with the degree of cell hyperpolarization. Following these current injections, the membrane potential *overshoots* the original resting potential and then slowly decays (dashed arrow). *B*, perforated patch recording in bath solution lacking TTX demonstrates that the overshoot following a sustained hyperpolarizing current injection can be of sufficient amplitude to trigger action potential firing (action potential amplitude has been truncated).

Instantaneous and time-dependent inward current components

Isolated SCP neurons exhibit a complex response to hyperpolarization. Under current clamp, small hyperpolarizing current injections cause membrane potential changes that are maintained for the duration of the current pulses. Contrastingly, larger current injections give rise to an initial hyperpolarization that is followed by

a slow *sag* of the membrane potential to a less hyperpolarized level (Fig. 2). In Fig. 2*A*, a depolarizing sag of a few millivolts is apparent over the course of several hundred milliseconds during small hyperpolarizations to potentials between −60 and −70 mV. During larger hyperpolarizations, both the amplitude and the initial

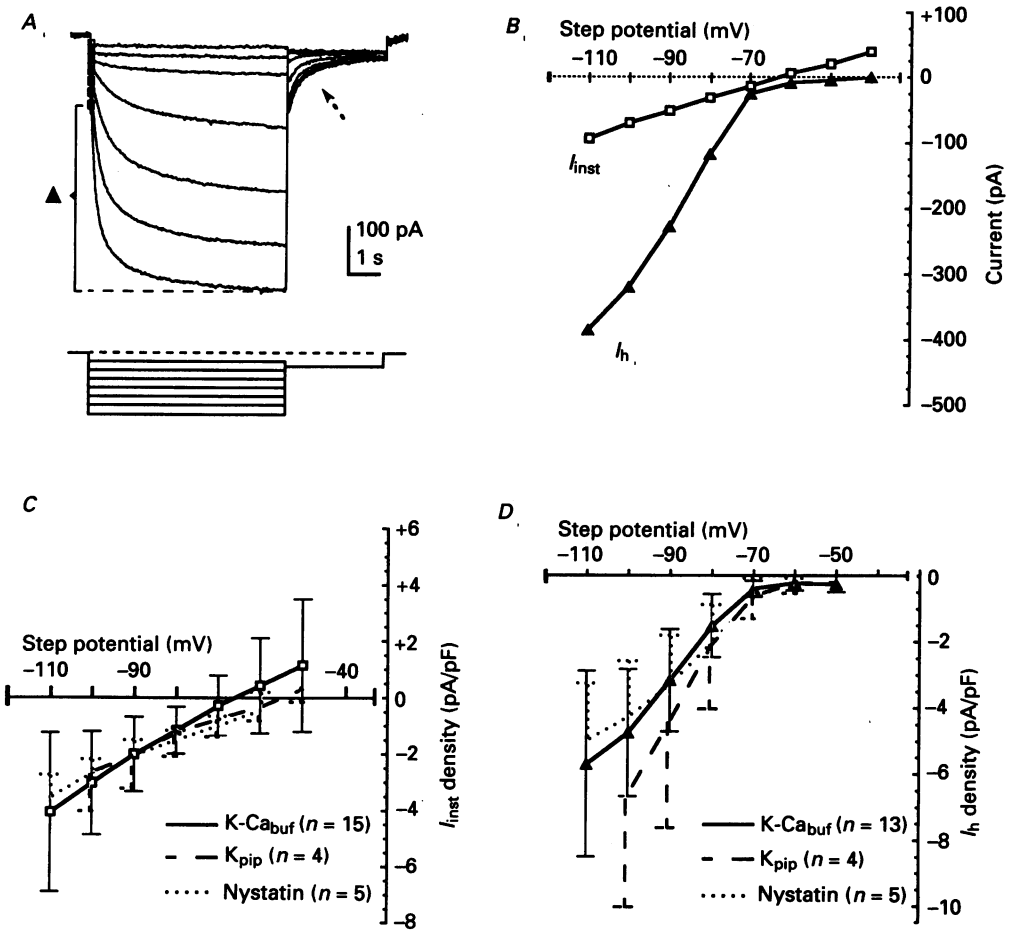

Fig. 3. I_{inst} and I_h in dissociated SCP neurons. *A*, in this whole-cell voltage clamp recording, hyperpolarizations from a holding potential of −40 mV evoke an instantaneous inward shift in voltage clamp current, I_{inst} (□). Voltage steps to potentials negative to −60 mV also elicit a slowly activating inward current, I_h (▲). Return of the membrane potential to −55 mV reveals inward tail currents (dashed arrow) that appear over the voltage range of I_h activation and whose peak amplitude reaches a maximum following hyperpolarizations to −100 mV. *B*, current *vs.* voltage relationships for I_{inst} (□) and I_h (▲) measured as illustrated in *A*. Mean (±S.D.) current density *vs.* voltage relationships for I_{inst} (*C*) and I_h (*D*) measured with intracellular free calcium concentration buffered to 100 nM with Ca-EGTA pipette solution (K-Ca$_{buf}$, continuous line), nominally Ca^{2+}-free pipette solution containing 10 mM EGTA (K$_{pip}$, dashed line), or the nystatin perforated patch technique (nystatin, dotted line).

rate of the voltage sag increase. Following cessation of large hyperpolarizing current injections, the membrane potential overshoots the original resting membrane potential and then decays back to rest over a long time course. This overshoot is often of sufficient magnitude to trigger the firing of one or more action potentials as illustrated in Fig. 2*B* (see also below).

Under voltage clamp, hyperpolarizations reveal the presence of two current components that could contribute to the complex response to hyperpolarizing current injections (Fig. 2). From a holding potential of −40 mV, hyperpolarizing voltage steps reveal an instantaneous, non-inactivating inward shift in voltage clamp current (I_{inst}). Voltage steps to potentials negative to −60 mV elicit an additional slowly activating inward current component that reaches a plateau over several hundred milliseconds (Fig. 3*A*). Similar hyperpolarization-activated inward currents, first described in photoreceptors (Fain, Quandt, Bastian & Gerschenfeld, 1978; Bader, MacLeish & Schwartz, 1979; Atwell & Wilson, 1980) have now been characterized in a wide variety of neuronal cell types (Mayer & Westbrook, 1983; Spain, Schwindt & Crill, 1987; Angstadt & Calabrese, 1989), as well as in pacemaker cells of the mammalian heart (Brown, DiFrancesco & Noble, 1979; Yanagihara & Irisawa, 1980; DiFrancesco, 1982). By analogy to other neuronal cell types, we refer to the time-dependent inward current in superior colliculus projecting visual cortical neurons as I_h.

The densities of I_{inst} and I_h at test potentials between −50 and −110 mV are shown in Fig. 3*C* and *D*. Current density in each cell was calculated by division of the current amplitude, measured at each test potential (Fig. 3*B*), by the cell capacitance (see Methods). As is evident, I_h densities are low with a mean current density (±S.D.) of −4·7 ± 1·9 pA/pF at −100 mV (n = 12). There is large cell-to-cell variability in the densities of both I_{inst} and I_h. Nevertheless, experiments completed to date reveal that, in general, I_h is larger than I_{inst}. Thus, I_h is the major component of the total steady-state inward current recorded at −80 mV or more negative potentials in SCP neurons (data not shown).

The hyperpolarization-activated current in rabbit sino-atrial node cells, termed I_f, is sensitive to the intracellular calcium concentration: between 1 and 100 nM there is a rightward shift in the voltage dependence of activation and up to a twofold increase in density, as estimated from the fully activated current tails (Hagiwara & Irisawa, 1989). To control for possible modulatory effects of variations in intracellular calcium, therefore, initial experiments were performed with a pipette solution in which intracellular free calcium was buffered to 100 nM with EGTA (K-Ca_{buf}). Nevertheless, subsequent experiments revealed that the densities of I_{inst} and I_h (Fig. 3*C* and *D*) were indistinguishable using K-Ca_{buf}, 10 mM EGTA pipette solution (K_{pip}), or the nystatin perforated patch recording technique (t test with Bonferroni correction). In spite of the scatter in the data, these analyses also revealed that I_h densities determined for cells studied with the K-Ca_{buff} and the 10 mM EGTA pipette solutions do not differ by more than 10% (95% confidence limits). I_h in SCP neurons, therefore, does not appear to possess the sensitivity to changes in intracellular calcium of sino-atrial node I_f.

Voltage dependences of I_{inst} *and* I_h

The current *versus* voltage (*I–V*) relationships for I_{inst} and I_h can be better appreciated in the normalized *I–V* curves shown in Fig. 4. At potentials negative to −40 mV, I_{inst}, recorded under whole-cell recording conditions, has a nearly linear

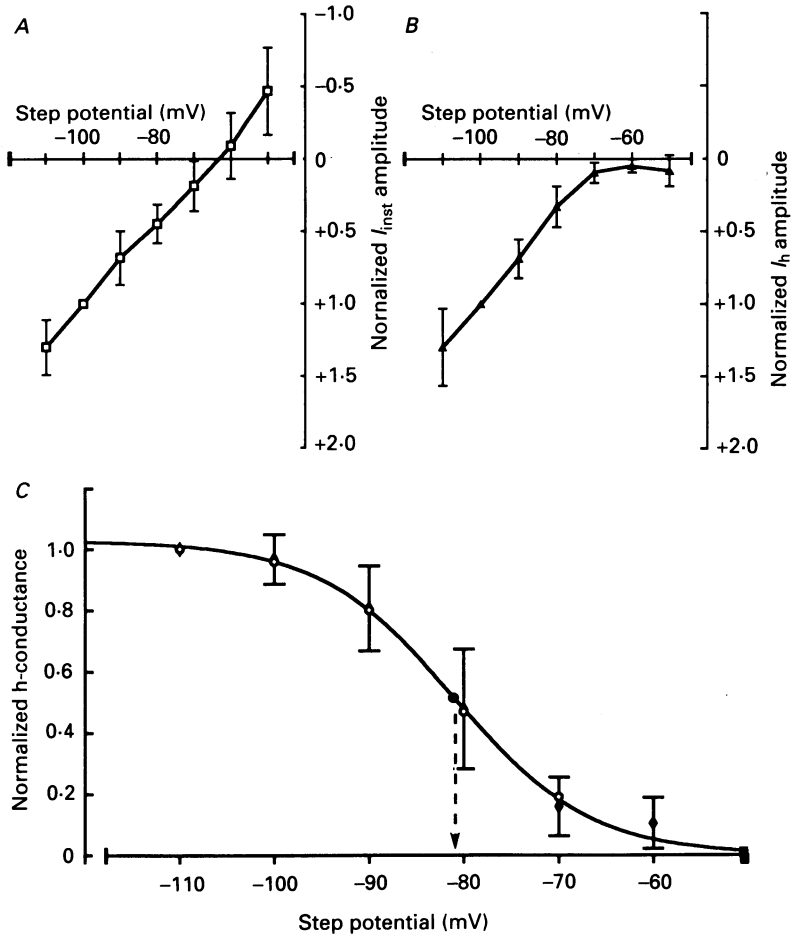

Fig. 4. Voltage dependences of I_{inst} (*A*) and I_h (*B*). I_{inst} and I_h in individual cells were measured (as illustrated in Fig. 3*A*) at each test potential and normalized to their respective values at −100 mV. Normalized data were then averaged over eleven cells. *C*, conductance *vs.* voltage relationship for I_h was determined in each of seven whole-cell recordings by dividing the amplitude of I_h by the h-current driving force (eqn (3)) with E_{rev} set equal to −21·5 mV (normal bath solution), and then normalizing to the value calculated for g_h at −110 mV. The data (◆) were well fitted by a single Boltzmann equation (see text) with $V_{\frac{1}{2}} = -81$ mV (indicated by ●) and $s = 7{\cdot}2$ ($r = 0{\cdot}98$). Tail current amplitudes in Fig. 3*A*, normalized to the tail amplitude measured at −110 mV (○), are also well described by the fitted curve.

I–V relation that intersects the voltage axis at the average zero-current potential of −63 mV (Fig. 4*A*). I_h begins to activate between −60 and −70 mV and the I–V relation is linear beyond −90 mV (Fig. 4*B*). Thus, I_h may be partially activated at rest and appears to reach full activation near −90 mV.

The voltage dependence of I_h activation was examined in greater detail by analysis of the chord conductance (g_h) *versus* voltage relationship. The magnitude of g_h at each step potential was calculated as:

$$g_h = \frac{I_h}{V - E_h}, \tag{3}$$

where V is the step potential and E_h is the I_h reversal potential. The conductance at each test potential was then normalized to the value at −110 mV for the same cell. E_h was estimated to be −21·5 mV (see Fig. 6). Mean normalized data from seven cells are plotted in Fig. 4*C* and fitted to a Boltzmann equation of the form:

$$g_h = \frac{g_{h,max}}{1 + e^{[(V - V_{\frac{1}{2}})/s]}}, \tag{4}$$

where $g_{h,max}$ is the maximum normalized conductance, $V_{\frac{1}{2}}$ is the membrane potential at which g_h is 50% of its maximum value, and s is a parameter that describes the steepness of the curve. The data are well fitted ($r = 0{\cdot}98$) by a single Boltzmann function with $V_{\frac{1}{2}}$ (±S.E.M.) = −81·0 ± 1·2 mV and s (±S.E.M.) = 7·2 ± 1·1 mV. The magnitude of g_h would, therefore, be approximately 5% of $g_{h,max}$ at −60 mV and 18% of $g_{h,max}$ at −70 mV. Thus, the h-conductance is activated over the range of SCP resting membrane potentials and is steeply voltage dependent. Under these ionic conditions ($[K^+]_o$ = 4 mM), g_h was maximal at −110 mV with a mean (±S.D.) value of 2·27 ± 1·31 nS.

I–V properties of the activated g_h

The results presented above suggest that the inward rectification of the whole-cell I–V curve can be accounted for by the voltage dependence of g_h activation. Tail current experiments were performed to determine if the activated conductance, itself, is rectifying. In these experiments, I_h was activated by a 3 s step to −100 mV, after which the cell was stepped to a test potential between −90 and +20 mV. Contaminating capacitative and ionic currents were isolated and subtracted off line using a paired pre-pulse protocol in which steps to the given test potential were preceded by only a 20 ms step to −100 mV, a period too brief to allow substantial activation of I_h (see Fig. 3*A*). As shown in Fig. 5*B*, the I–V relation for the activated g_h is nearly linear. Assuming that Na^+ and K^+ are the only permeant species and that their flux through g_h obeys independence (see below), the slight curvature can be accounted for by constant field rectification according to the Goldman–Hodgkin–Katz current equation (Goldman, 1943; Hodgkin & Katz, 1949):

$$I_h = P_K \frac{VF^2}{RT} \frac{[K^+]_i - [K^+]_o e^{(-VF/RT)}}{1 - e^{(-VF/RT)}} + P_{Na} \frac{VF^2}{RT} \frac{[Na^+]_i - [Na^+]_o e^{(-VF/RT)}}{1 - e^{(-VF/RT)}}, \tag{5}$$

where P_X is the permeability of ion X, V is the membrane voltage, $[X]_i$ and $[X]_o$ are the intracellular and extracellular ion concentrations respectively, and F, R, and T

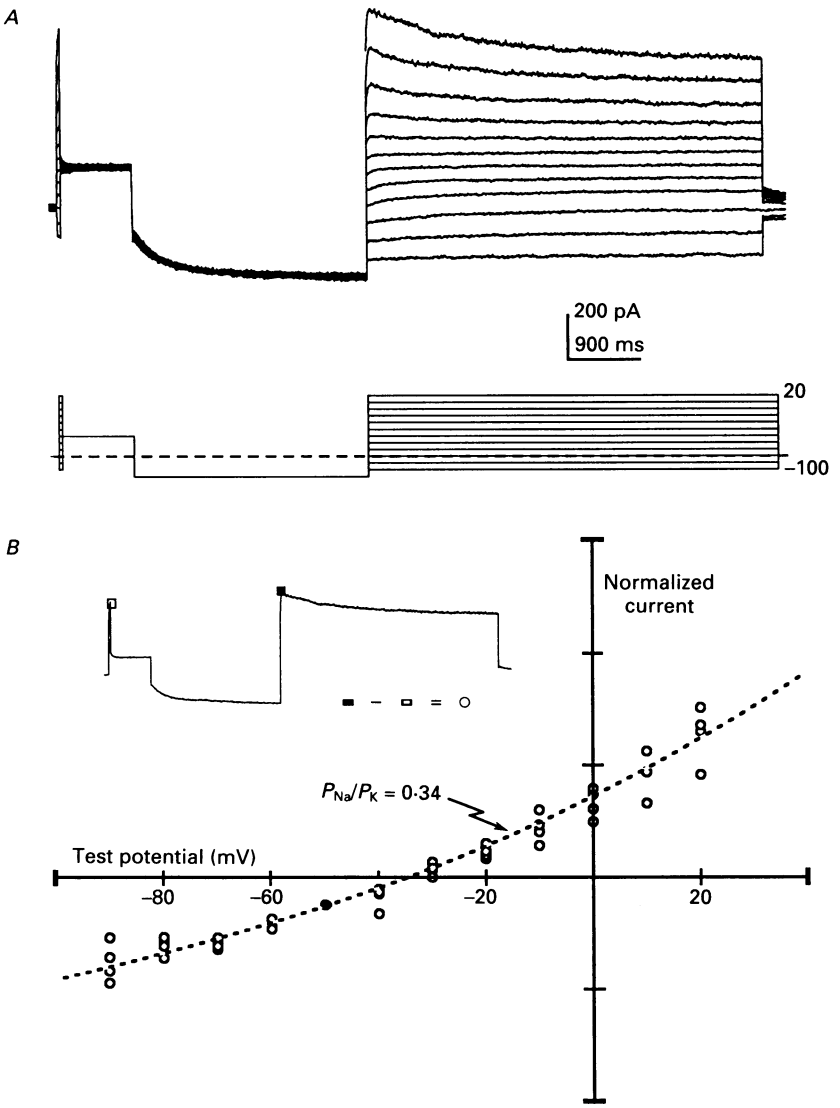

Fig. 5. Currents through activated g_h. *A*, in 100 mM Na^+ bath solution, whole-cell currents were recorded during voltage steps to various test potentials between −90 and +20 mV which were preceded by long hyperpolarizing steps to −100 mV to activate g_h (see protocol). Contaminating capacitative and ionic currents were determined during a series of pre-pulses to the various test potentials preceded by only a 20 ms step to −100 mV (see protocol), a period too brief to activate g_h substantially. Contaminating currents were then subtracted off-line. *B*, current through activated g_h *vs.* voltage. The inset is a diagram of the subtraction procedure for isolation of I_h from contaminating ionic and capacitative currents. In individual cells ($n = 5$), the subtracted current amplitudes at each test potential were normalized to the amplitude recorded during the step to −50 mV in the same cell. The current *vs.* voltage relationship is nearly linear, showing slight outward rectification that is accounted for by constant field considerations (see text). The data were best fitted ($r = 0{\cdot}92$) to the Goldman–Hodgkin–Katz current equation (eqn (5)) with $P_{Na}/P_K = 0{\cdot}34$ (dashed line). Linear interpolation between the current amplitudes recorded at −30 mV and −40 mV indicates an I_h reversal potential of −33 mV.

have their usual meanings. The conductance, g_h, therefore, appears to have no intrinsic rectifying properties. Furthermore, under the ionic conditions used, the reversal potential (E_{rev}), defined by the intersection of the I–V curve with the voltage axis, is approximately −33 mV and is, thus, well depolarized from rest. Consequently, once activated, I_h will exert a depolarizing influence on SCP neurons at all membrane potentials more hyperpolarized than the reversal potential until deactivation is complete.

Relative ion permeabilities of g_h

Use of the whole-cell patch clamp technique allows stringent control of intracellular and extracellular ion concentrations. Because none of the ions in our recording solutions (Table 1) are present in concentrations that would give rise to a reversal potential of −33 mV, g_h, if non-electrogenic, must be permeable to a combination of ions whose individual reversal potentials lie on either side of this value. Indeed, I_h-like currents in other systems have been described as mixed sodium–potassium currents (DiFrancesco, 1981; Hestrin, 1987; Spain *et al.* 1987).

Altering extracellular sodium or potassium concentration had profound effects on I_h amplitude and reversal potential. To examine the relative permeabilities of sodium and potassium in greater detail, a series of experiments was performed in which the I_h reversal potential was determined (see Fig. 5*B*), while varying extracellular sodium and/or potassium ion concentrations. The reversal potentials, calculated from the resultant I–V curves by linear interpolation between the voltage steps straddling zero current, are plotted in Fig. 6. For a conductance that is permeable to monovalent ions, the relationship between permeant ion concentration and reversal potential at 20 °C, assuming a constant electrical field and independence of ion flow, is described by the Goldman–Hodgkin–Katz voltage equation (Goldman, 1943; Hodgkin & Katz, 1949):

$$E_{rev} = 25{\cdot}3 \ln\left(\frac{P_K[K^+]_o + P_{Na}[Na^+]_o + P_{Cl}[Cl^-]_i}{P_K[K^+]_i + P_{Na}[Na^+]_i + P_{Cl}[Cl^-]_o}\right), \quad (6)$$

in which all symbols have the same meaning as described in eqn (5). Ignoring for the moment any contribution from chloride ions (see below), calculations of the I_h reversal potential suggest that, over a broad range of extracellular sodium and potassium ion concentrations, I_h can be modelled as arising from the independent movement of sodium and potassium ions. For $[K^+]_o \leqslant 20$ mM and $[Na^+]_o$ between 70 and 120 mM, the reversal potential of I_h was well described by the Goldman–Hodgkin–Katz voltage equation (eqn (6)) with $P_{Na}/P_K = 0{\cdot}40 \pm 0{\cdot}085$ ($n = 38$). Over this concentration range, there was no significant effect of changing sodium or potassium concentration on P_{Na}/P_K (ANOVA and Newman–Keuls tests). At physiological ion concentrations, therefore, I_h would be expected to reverse at −21·5 mV. Because of the need for 20 mM extracellular TEA in these experiments to block depolarization-activated outward K^+ currents, the reversal potential at physiological concentrations of extracellular sodium and potassium could not be determined directly without increasing the osmolarity of the solution. Although variations in extracellular $[Na^+]$ and $[K^+]$ near physiological concentrations are well described by the surface in Fig. 6, ion movement through g_h following more extreme

changes in the concentrations of these ions clearly deviates from the predictions of eqn (6) (independence), suggesting some ion interaction within h-channels. Deviations were consistently in the direction of an increase in P_{Na}/P_K (Edman, Gestrelius & Grampp, 1987).

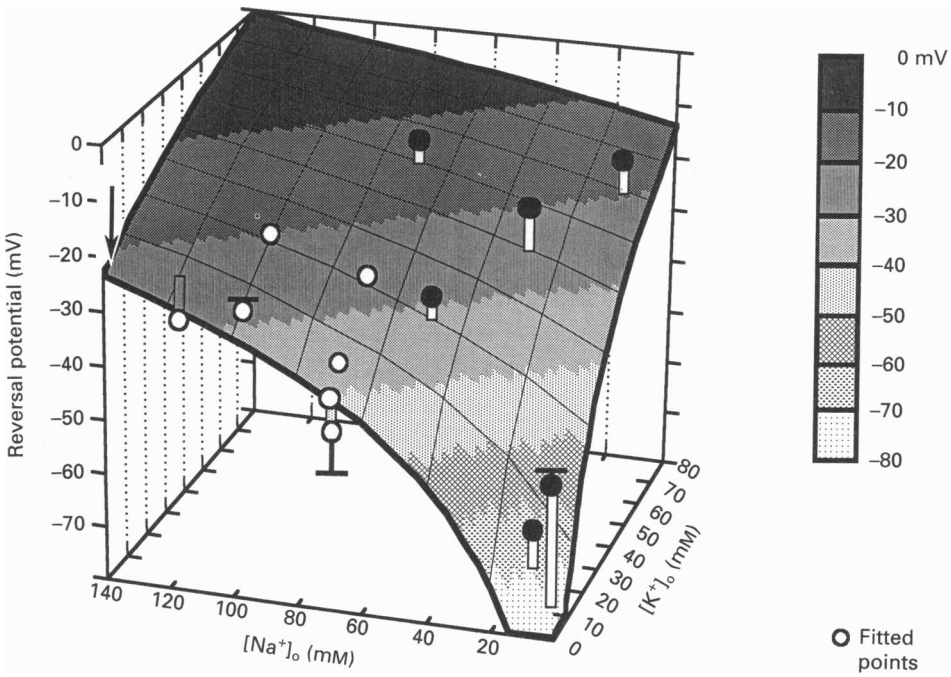

Fig. 6. Change in I_h reversal potential as a function of extracellular $[Na^+]$ and $[K^+]$. Each point (○, ●) represents the mean of the reversal potentials determined in three to ten cells by linear interpolation (as in the legend of Fig. 5*B*). For three points, standard error bars were larger than the symbol size and are indicated. P_{Na}/P_K ratios were calculated according to eqn (6) (see text) and, for points (○) close to physiological Na^+ and K^+ concentration (arrow), were not significantly different from one another (ANOVA, Newman–Keuls) having a mean value of 0·40. The fitted surface represents the solution to the Goldman–Hodgkin–Katz voltage equation for a conductance that obeys independence (eqn (6)) and is permeable only to Na^+ and K^+ with $P_{Na}/P_K = 0{\cdot}4$. The location of each point with respect to the *z*-axis, indicated by the degree of shading surrounding the point, reflects the observed reversal potential. Bars extending from the points reflect distance above (open bars) or below (filled bars) the surface and, thus, contact the surface at the location determined by the extracellular Na^+ and K^+ concentrations used. The increase in P_{Na}/P_K during more extreme changes in ion concentration (●) suggest ion–ion interactions and/or the existence of ion binding sites within the channel pore.

The potential contribution of chloride ions to I_h was more difficult to ascertain. Similar to previous reports (Mayer & Westbrook, 1983; McCormick & Pape, 1990), we found that replacement of chloride with impermeant anions caused a decrease in current amplitude (Fig. 7*A* and *B*); however, it was unclear whether this response was due to a contribution of chloride to the current or simply the result of a blocking action of the anion substitute. Clearly, the decrease of I_h, as well as the alterations

in tail current waveforms, during puffer application of bath solution containing 140 mM sodium isethionate reflects some direct effects of isethionate on h-channel gating. If chloride were permeant and isethionate were not blocking, such a replacement of extracellular chloride would have been expected to increase the

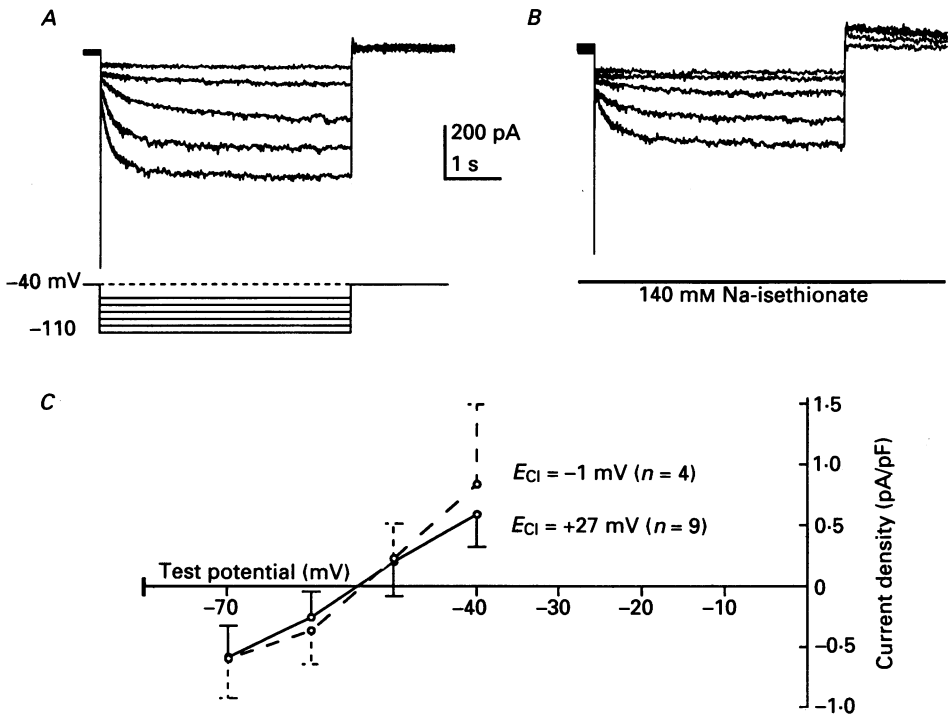

Fig. 7. Effect of changes in extracellular chloride on I_h. *A*, whole-cell h-currents recorded under voltage clamp in normal bath solution. *B*, continuous puffer application of 140 mM Na-isethionate to the cell shown in *A* caused a pronounced decrease of I_h; the current recovered rapidly after puffing was discontinued (not shown). *C*, mean I_h density *vs.* voltage relationships for the activated conductance in 10 mM Na^+ and ΔCl bath solutions. As is evident, g_h is unaffected by replacement of 200 mM sucrose (continuous line) with 100 mM choline chloride (dashed line). Although the chloride equilibrium potential changes from −1 mV (dashed line) to +27 mV (continuous line), the reversal potential for I_h remains unchanged at ≈ -53 mV.

driving force for chloride efflux and, consequently, *increase* h-current amplitude. To further examine whether chloride can permeate I_h channels, therefore, the I_h reversal potential was determined in two 10 mM Na^+ bath solutions containing differing concentrations of chloride. Corresponding changes in the I_h reversal potential (eqn (6)) following alteration of the chloride equilibrium potential would indicate that chloride can permeate the h-conductance, provided the experimental solutions used did not, themselves, alter the permeability properties of the channels. Reduced extracellular concentrations of the demonstrably permeant ions, sodium and potassium, were used to detect minor permeant ionic species more readily. As shown in Fig. 7*C*, the activated h-current density *vs.* voltage relationship was unchanged when sucrose was replaced by choline chloride, indicating that this solution change,

unlike that of replacing sodium chloride with sodium isethionate, did not substantially alter the permeability properties of I_h channels. Moreover, despite variation in the chloride equilibrium potential between -1 and $+27$ mV, the I_h reversal potential remained unchanged at ≈ -53 mV ($-51{\cdot}7 \pm 2{\cdot}8$ mV and $-54{\cdot}4 \pm 5{\cdot}9$ mV, respectively). With 95% confidence, the 28 mV increase in E_{Cl} resulted in a maximum increase in reversal potential of 1·5 mV. Substitution of this value for ΔE_{rev} into eqn (6) gives:

$$\Delta E_{rev} > 25{\cdot}3 \ln\left(\frac{P_K[K^+]_{i,1} + P_{Na}[Na^+]_{i,1} + P_{Cl}[Cl^-]_{o,1}}{P_K[K^+]_{i,2} + P_{Na}[Na^+]_{i,2} + P_{Cl}[Cl^-]_{o,2}}\right),$$

where $[X]_{o,1}$ and $[X]_{o,2}$ are the concentrations of ion X in bath solution 1 and bath solution 2, respectively, and all other symbols have their previously defined meaning. Solving this equation:

$$\frac{P_{Cl}}{P_K} < 9{\cdot}9 \times 10^{-4} \frac{P_{Na}}{P_K} + 0{\cdot}09.$$

Thus, for all realistic values of P_{Na}, the maximum chloride permeability through g_h is approximately $0{\cdot}09 \times P_K$. The quality of the fits in Figs 5*B* and 6 was not substantially altered by the inclusion of a chloride/potassium permeability ratio of 0·09.

The possibility that h-channels have measurable permeability to ions other than sodium and potassium was examined by further ion substitution experiments. The addition of 5 mM $CoCl_2$ to normal bath solution at a concentration sufficient to block voltage-activated calcium currents, had no measurable effects on I_h amplitudes or waveforms, although the voltage dependence of I_h activation was shifted by $+6$ mV (data not shown). Recordings were also obtained in which all sodium chloride and potassium chloride, both intracellular and extracellular, were replaced with choline chloride. The average time-dependent current density in two of seven cells was $-2{\cdot}2$ pA/pF at -100 mV with no measurable current in the remaining five of seven cells. Taken together, these results indicate that calcium and magnesium also have little, if any, permeability through g_h under the conditions of these experiments.

In the course of the above permeability experiments, we observed that the amplitude of I_h at a given test potential was much larger when extracellular potassium was increased. To examine the effect of extracellular potassium on I_h amplitudes independent of its effects on I_h reversal potential, the magnitude of the h-conductance in individual cells was assessed in a static bath of a particular ΔK^+ solution (see Table 1). The zero-current conductance ($G_{h,0}$), was determined by measuring the slope of the h-current *versus* voltage relationship in the region of its intersection with the voltage axis; $G_{h,0}$ was then normalized to cell capacitance ($\bar{G}_{h,0}$). A plot of normalized conductance *versus* extracellular potassium concentration is shown in Fig. 8. The effects of extracellular potassium on $\bar{G}_{h,0}$ were modelled as resulting from the binding of potassium ions to an extracellular conductance-permitting site. The data were fitted to a Michaelis–Menten-type rectangular hyperbola:

$$\bar{G}_{h,0} = \bar{G}_{h,0,max} \frac{[K^+]_o}{[K^+]_o + K_{app}}, \quad (7)$$

where $\bar{G}_{h,0,max}$ is the maximum normalized conductance, $[K^+]_o$ is the extracellular potassium concentration, and K_{app} is the apparent dissociation constant for the potassium binding site. Despite the normalization to cell capacitance, there is a great deal of variability in the conductance measurements ($r = 0{\cdot}76$). None the less, the

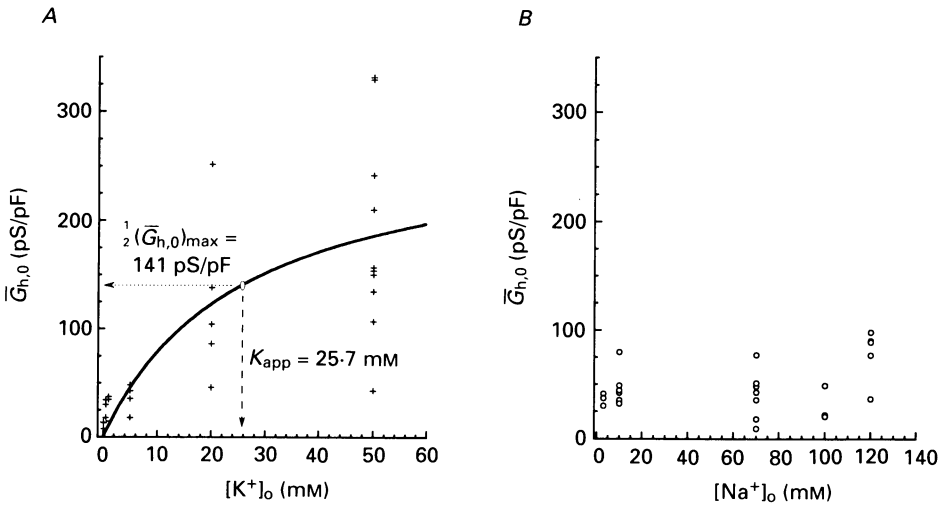

Fig. 8. Changes in extracellular potassium alter g_h. The zero current h-conductance ($G_{h,0}$) was determined by measuring the slope of the activated whole-cell current *vs.* voltage relationship in the region of the reversal potential in various ΔK (*A*) and ΔNa (*B*) bath solutions (see Table 1). Conductance values were then normalized to cell capacitance measurements. *A*, each (+) represents a conductance measurement from a different cell. Increases in $[K^+]_o$ up to 50 mM cause large increases in normalized $G_{h,0}$ ($\bar{G}_{h,0}$). The continuous line represents the best fitting Michaelis–Menten-type rectangular hyperbola (eqn (7)) and indicates that the half-maximal activation of the normalized conductance of 141 pS/pF (dotted line) occurs at a $[K^+]_o$ of 25·7 mM (dashed line). Although there is considerable scatter in the data ($r = 0{\cdot}76$), it is clear that normalized $G_{h,0}$ is modulated by small alterations in $[K^+]_o$ near the physiological range. *B*, there is no correlation between normalized $G_{h,0}$ and $[Na^+]_o$.

data suggest that extracellular potassium may be necessary for ion flux through h-channels and that the putative permissive site has a mean (±S.E.M.) apparent dissociation constant for potassium ion of 25·7 ± 7·6 mM. The maximal whole-cell normalized h-conductance (±S.E.M.) is 281·5 ± 23·0 pS/pF ($n = 27$). The best fit parameters to this model, therefore, predict an approximately ±20% variation in $\bar{G}_{h,0}$ as a result of only a 1 mM change in extracellular potassium about the physiological concentration of 3–4 mM. In contrast, changes in extracellular sodium concentration in the presence of 5 mM potassium were not significantly correlated with changes in $\bar{G}_{h,0}$ (Fig. 8*B*) as determined by linear regression analysis of a double reciprocal (Lineweaver–Burk) plot (not shown).

Block of I_h by extracellular Cs^+

Hyperpolarization-activated currents similar to I_h (DiFrancesco, 1982), as well as the very different inward rectifier current in starfish oocytes (Hagiwara, Miyazaki & Rosenthal, 1976), are blocked by the extracellular application of 3 mM CsCl. Puffer

application of 3 mM CsCl to SCP neurons (Fig. 9) eliminates the time-dependent component of the current. Digital subtraction of the Cs^+-blocked from the control current records indicates that the Cs^+-sensitive component is the slowly activating, non-inactivating inward current, I_h. Extracellular Cs^+ thus blocks I_h without

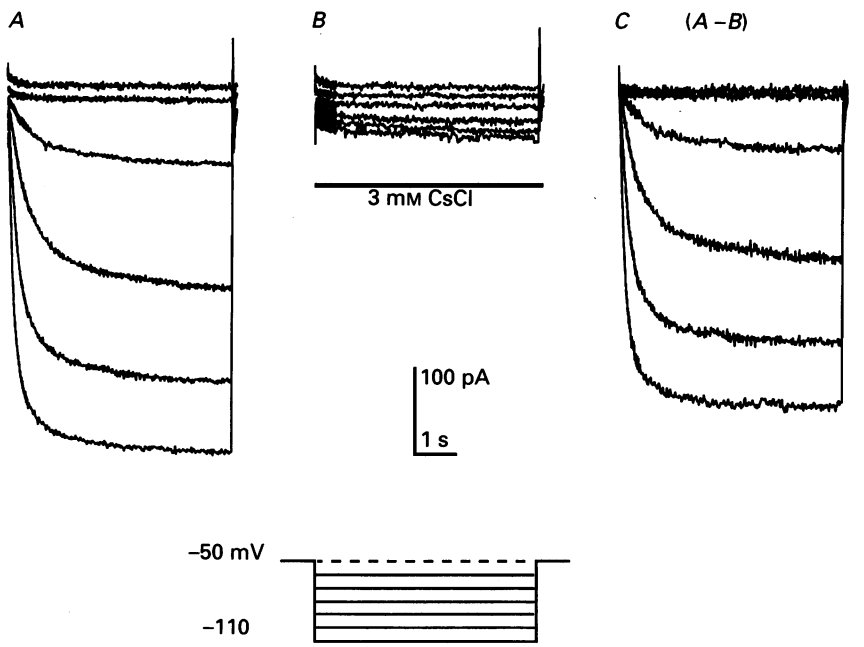

Fig. 9. Low concentrations of extracellular caesium selectively block I_h. *A*, in this perforated patch recording, voltage steps to hyperpolarized potentials elicit typical I_{inst} and I_h. *B*, repetition of the voltage clamp protocol during continuous puffer application of 3 mM CsCl blocks I_h, while the low amplitude I_{inst} in *A* is unaffected. *C*, digital off-line subtraction of the traces in *B* from the traces in *A* reveal that the Cs^+-sensitive current component is the slowly activating inward current, I_h.

affecting I_{inst}. Extracellular applications of 3 mM CsCl during depolarizing test pulses had no measurable effect on depolarization-activated outward potassium currents in SCP cells (data not shown).

Under current clamp recording conditions, CsCl has three major effects (Fig. 10). At rest, puffer application of 3 mM Cs^+ can cause some degree of cell hyperpolarization due to the block of h-channels that are activated at rest. During hyperpolarizing current injections, Cs^+ eliminates both the sag and the overshoot (Fig. 2). The initial hyperpolarization at the beginning of the current pulse remains relatively unchanged. Rather than sagging back to a more depolarized level, however, the initial level of hyperpolarization is maintained for the duration of the current pulse. Caesium, thus, has the net effect of substantially increasing the steady-state input resistance of the cell over the voltage domain of I_h activation; hyperpolarizing current injections of a given magnitude now give rise to much larger steady-state hyperpolarizations. Despite the increased amplitude of the hyperpolarization, however, there is no overshoot of the resting potential following the current pulse, due to block of I_h.

Functional role of I_h

Taken together, the results presented above suggest that I_h contributes to setting the resting membrane potential of SCP neurons and underlies the sag and overshoot phenomena in these cells (see also Fig. 2). In addition, the results above suggest that

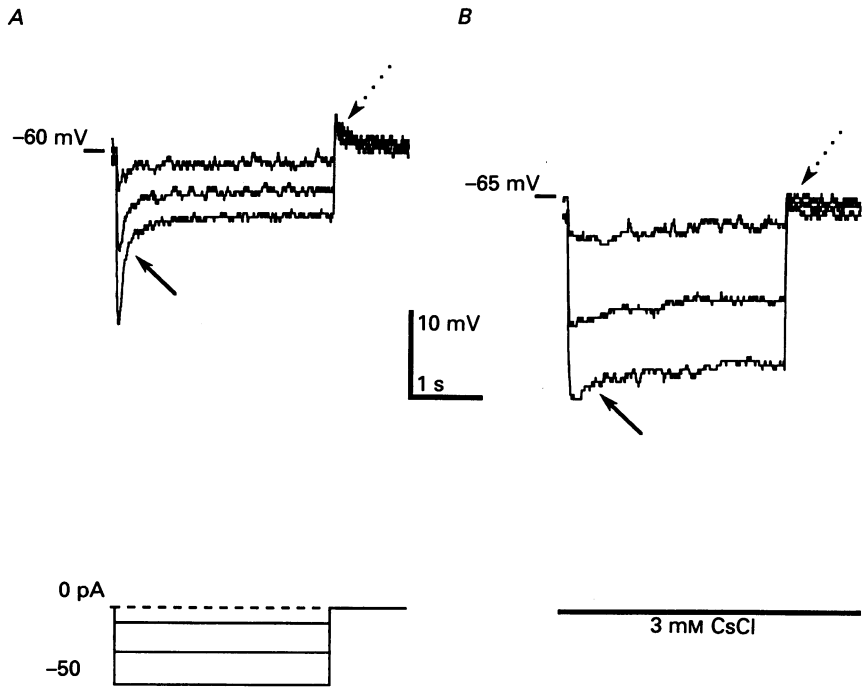

Fig. 10. Low concentrations of extracellular caesium block the *sag* and *overshoot*. *A*, whole-cell recording showing that hyperpolarizing current injections of sufficient magnitude cause a rapid change in SCP membrane potential that is followed by a slow depolarizing sag to a new steady-state membrane potential (continuous arrow); see also Fig. 2. Following the current injection, the membrane potential transiently overshoots the original rest potential and then slowly decays back (dashed arrow). *B*, repeating the protocol on the cell shown in *A* during continuous puffer application of 3 mM CsCl virtually eliminates the sag and overshoot. Initial application of 3 mM CsCl causes a slight hyperpolarization, reflecting the block of inward h-current in this cell at rest. Hyperpolarizing current injections now lead to rapid changes in membrane potential with little or no sag (continuous arrow). In addition, following the hyperpolarizing current injections, there is no overshoot (dashed arrow).

I_h may also be important in mediating the rebound firing of action potentials following cell hyperpolarization (as seen, for example, in Fig. 2*B*). Therefore, subsequent experiments were aimed at determining the relationship between I_h activation and the generation of rebound firing in SCP neurons. Under current clamp, however, the degree of activation of g_h is difficult to control due to time-dependent changes in membrane voltage. To circumvent this problem, experiments were conducted using a switch clamp (see Methods). This technique permits precise control of the degree of I_h activation under voltage clamp prior to measurements of

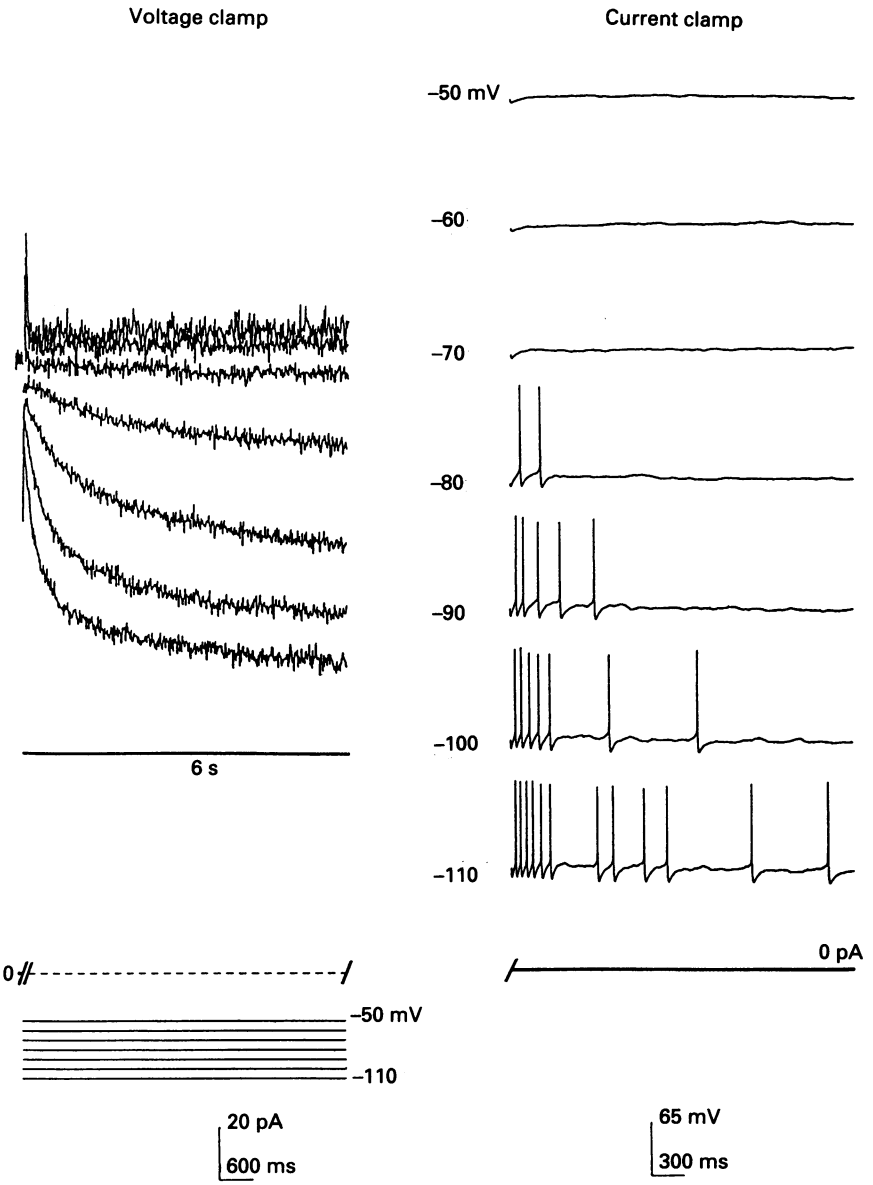

Fig. 11. Post-hyperpolarization repetitive firing is correlated with the activation of I_h. Nystatin perforated patch voltage (left panel) and current (right panel) clamp recordings in normal bath solution (Table 1). I_h waveforms were recorded during 6 s hyperpolarizing voltage steps to potentials between −50 and −110 mV from a holding potential of −40 mV. At the end of each voltage step, the cell was switched to current clamp mode and the voltage recordings were begun immediately (right panel). The numbers on the left of each voltage record indicate the potential to which the cell was clamped prior to switching to current clamp mode. Following steps to −80 mV or more negative potentials, the cell fires action potentials on switching to current clamp mode. In addition, the rate and duration of repetitive firing increase following voltage steps to the more hyperpolarized test potentials.

membrane potential under current clamp. Data obtained in one such experiment are presented in Fig. 11. In the left panel, I_h waveforms, evoked during hyperpolarizing voltage steps from a holding potential of −40 mV, are displayed; in the right panel are the corresponding membrane potential records obtained following rapid

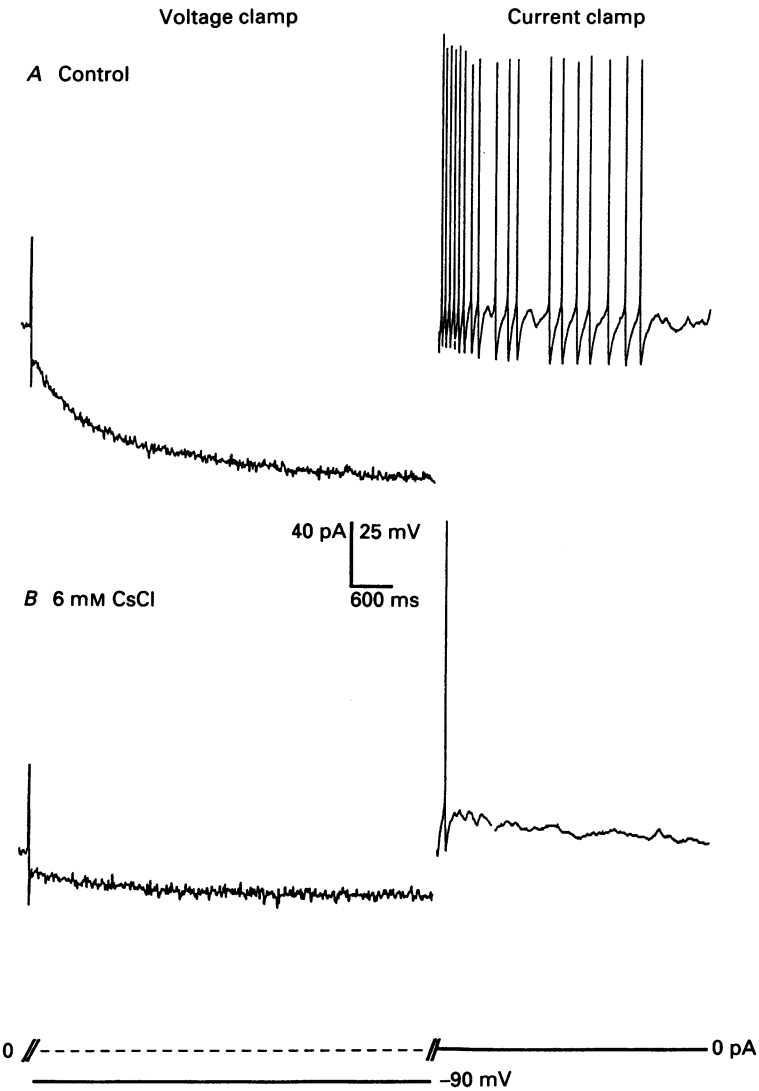

Fig. 12. Low concentrations of caesium block I_h and post-hyperpolarization repetitive firing. *A*, control voltage (left panel) and current (right panel) clamp perforated patch recordings from an isolated SCP neuron. Prior hyperpolarization of this cell to −90 mV for 6 s results in repetitive firing on switching to the current clamp mode. *B*, voltage and current clamp records from the same cell as in *A* except that these records were obtained in the presence of 6 mM extracellular caesium. As is evident, I_h amplitude is decreased compared to control (left panel) and only a single action potential was fired on switching to the current clamp mode (right panel).

switching to the current clamp mode. Action potentials were first observed following a hyperpolarization to −80 mV. When the size of the hyperpolarizing voltage step was increased, both the frequency and the duration of repetitive firing increased. This post-hyperpolarization repetitive firing was blocked by extracellular application of caesium (Fig. 12), suggesting an important role for I_h in mediating this activity.

DISCUSSION

Properties of SCP neurons

Retrograde labelling experiments have demonstrated the existence of at least two anatomically and morphologically distinct types of pyramidal neurons residing in layer 5 of rat visual cortex: cortico-cortical neurons that project to ipsilateral and contralateral visual areas, and subcortically projecting neurons whose axons extend to such structures as the superior colliculus and the pons (Hallman *et al.* 1988). Consistent with previous studies, retrogradely labelled SCP neurons were localized to cortical layer 5 (Hallman *et al.* 1988). These cells possessed large, gradually tapering apical dendrites that extend up to layer 1 and, thus, may be classified as *thick* layer 5 cells (Larkman & Mason, 1990). In recordings from slices of rat visual cortex, thick layer 5 cells are reported to be *intrinsic bursting* neurons, and these cells exhibit a prominent depolarizing sag and overshoot in response to a hyperpolarizing current injection (Mason & Larkman, 1990).

Hyperpolarization-activated current types

The instantaneous and time-dependent inward currents observed following voltage steps hyperpolarized from the resting membrane potential suggest the existence of at least two independent conductance pathways. At all test potentials, there is a caesium-resistant instantaneous inward current (I_{inst}). The current–voltage relationship for I_{inst} is nearly linear and may reflect the passage of current through multiple conductance pathways. The time-dependent currents recorded from SCP neurons during cell hyperpolarizations beyond approximately −60 mV appear to be similar to variously named hyperpolarization-activated currents recorded in other systems that, unlike traditional inward rectifier currents, are significantly permeable to sodium. Such currents were first identified in photoreceptors (Fain *et al.* 1978; Bader *et al.* 1979; Atwell & Wilson, 1980) and since then have been described in a number of different preparations (Yanagihara & Irisawa, 1980; DiFrancesco, 1981; Mayer & Westbrook, 1983; Spain *et al.* 1987). Similar to SCP neurons, the I_h currents in these cells also begin to activate between −45 and −60 mV and, generally, half-activation is seen between −75 and −85 mV, although closer to −65 mV in salamander rods (Hestrin, 1987). While the half-activation voltage for I_f in rabbit sino-atrial node has been reported in the range of −75 to −85 mV, more depolarized values have also been observed and attributed to a modulatory effect of increases in intracellular calcium (Hagiwara & Irisawa, 1989). In the experiments here, however, I_h amplitudes in SCP neurons were not measurably altered by varying intracellular calcium.

I_h amplitude

The amplitude of I_h varies markedly in isolated SCP neurons and, under physiological recording conditions, the mean maximal conductance is $2{\cdot}3 \pm 1{\cdot}3$ nS. Although the mean I_h at -90 mV is only -77 pA ($n = 46$), the density of I_h in dissociated SCP neurons (mean at -90 mV $= -3$ pA/pF) is comparable to the current densities reported for similar currents in other systems (Edman *et al.* 1987). If h-channels are uniformly distributed over the SCP cell surface, the amplitude of I_h *in vivo* could be much larger than the values reported here not only because of the 10–20-fold increase in cell membrane surface area (capacitance) of thick layer 5 cells in intact preparations (Mason & Larkman, 1990), but also as a result of the increase in diffusional flux that would be expected to accompany the warming of the preparation to physiological temperatures. Such increases in I_h amplitude should not, however, alter the suggestion that I_h underlies the sag and overshoot phenomena unless, of course, there are quite distinct changes in other membrane conductance pathways. Further experiments will be needed to explore this point.

h-Channel permeability characteristics

Similar to hyperpolarization-activated currents in other systems (DiFrancesco, 1981; Mayer & Westbrook, 1983; Edman & Grampp, 1989; Angstadt & Calabrese, 1989), I_h in SCP neurons is a mixed sodium and potassium conductance. It is not, however, a non-specific ion pore. G_h has a sodium:potassium permeability ratio of 2:5 that is maintained over a wide range of sodium and potassium concentrations. Furthermore, the conductance failed to demonstrate any measurable permeability to other cations, such as calcium or magnesium. Experiments aimed at examining the permeability of chloride through h-like channels have also been completed. Similar to results in other preparations (Mayer & Westbrook, 1983; McCormick & Pape, 1990), replacement of extracellular chloride with isethionate caused a decrease in h-current amplitude in SCP neurons. Because the current decreased in our experiments despite an increase in the inward driving force on chloride ions, these results suggest a blocking action of the anion substitute, isethionate. Additional experiments were performed, therefore, in which extracellular choline chloride was replaced with isosmotic sucrose. This manipulation had no effect on g_h and, despite a 28 mV change in E_{Cl}, had no significant effect on the I_h reversal potential, indicating that chloride has little, if any, permeability through h-channels. Although it is conceivable that chloride, like potassium, could have an activating effect, this hypothesis is not consistent with the observations that alterations in sodium and chloride by the replacement of NaCl with sucrose had no effect on normalized $G_{h,0}$, and that replacement of 200 mM sucrose with 100 mM choline chloride had no effect on activated I_h current density.

Although a previous study has modelled the passage of sodium and potassium ions through I_h-like channels using Eyring rate equations (Edman & Grampp, 1989), current flow through I_h channels in SCP neurons, over a broad range of sodium and potassium concentrations approaching the physiological range, appears to be adequately described by constant field theory (Goldman, 1943). Nevertheless, more complicated models such as that cited above may, indeed, be required to explain the

increase in P_{Na}/P_K observed during the more extreme changes in extracellular sodium and potassium ion concentrations.

Modulation by extracellular potassium

The magnitude of the h-conductance exhibits a strong dependence on the extracellular potassium concentration. The experimental observations are consistent with reported effects of extracellular potassium on inward current (DiFrancesco, 1981; Hestrin, 1987; Edman & Grampp, 1989; McCormick & Pape, 1990) and tail current (DiFrancesco, 1982; Hestrin, 1987; Edman & Grampp, 1989) amplitudes of similar hyperpolarization-activated currents in other systems. Our estimation of K_{app} to be $25{\cdot}7 \pm 7{\cdot}6$ mM potassium is comparable to the values of 35–50 mM K^+ reported for I_f in calf heart Purkinje fibres (DiFrancesco, 1982) and 20 mM K^+ for I_Q (hyperpolarization-activated membrane channels) in lobster stretch receptor neurons (Edman & Grampp, 1989). As can be seen in Fig. 8, there is a high degree of scatter in the data at the elevated potassium ion concentrations. A large portion of the scatter is likely to arise from cell-to-cell variability in $\bar{G}_{h,0}$, despite normalization of the conductance measurements to cell capacitance. A more detailed description of the effects of extracellular potassium on I_h might be obtained by examining the effects of multiple potassium ion concentrations on single neurons.

The model presented here for the existence of an extracellular, potassium-binding regulatory site predicts a variation of normalized $G_{h,0}$ between about 5 and 35% of its maximal value ($\bar{G}_{h,0,max}$) for extracellular potassium concentrations between 1 and 10 mM, respectively. Direct measurements of interstitial potassium concentration using ion-sensitive electrodes suggest that basal extracellular concentrations of potassium in the cerebral cortex of cat (Hotson, Sypert & Ward, 1973), rabbit (Futamachi, Mutani & Prince, 1974) and rat (Vyskočil, Kříž & Bureš, 1972), are 3–4 mM, similar to the potassium concentration in cerebrospinal fluid. Electrical stimulation of the cortex or penicillin-induced epileptic discharges reportedly raise interstitial potassium concentration up to 10 mM for periods of seconds. Such an increase in extracellular potassium would increase the basal h-conductance around twofold. Even larger increases in interstitial potassium concentrations have been observed in models of anoxia (Vyskočil *et al.* 1972; Ohno, Obrenovitch, Hartell, Barratt, Bachelard & Symon, 1989) and cerebral ischaemia (Schielke, Moises & Betz, 1991).

Interestingly, maximal increases in interstitial potassium concentration recorded during spontaneous *interictal* discharges from rabbit cortex (1–2 mM over basal levels) are localized to the deeper layers of cortex (Futamachi *et al.* 1974). Such alterations in local potassium concentration may, therefore, be particularly effective in modulating h-channels on the cell body and/or basal processes of layer 5 SCP neurons. The potential interrelationship of synchronized cortical electrical activity and augmentation of I_h in lower cortical layers is especially intriguing in light of recent work indicating that layer 5 cortical neurons may be essential in the generation of oscillating cortical field potentials (Silva, Amitai & Connors, 1991).

Functional role of I_h

The results here suggest that I_h may play an important role in regulating the firing properties of SCP neurons. The voltage dependence of current activation indicates that some I_h channels are likely to be open at the resting membrane potential with the conductance being 5–18% activated between −60 and −70 mV. I_h may, therefore, contribute to setting the resting membrane potential and controlling the input resistance in this voltage region.

A more important contribution of I_h, however, is expected to be its participation in the electrical response of SCP neurons to hyperpolarizing synaptic inputs. I_h is a slowly activating, non-inactivating inward current whose hyperpolarized voltage range of activation parallels the appearance of depolarizing sags and post-hyperpolarization overshoots under current clamp. Because the reversal potential for I_h is approximately −22 mV, the net inward sodium/potassium current exerts a time-dependent depolarizing influence on cells during (I_h activation) and following (I_h deactivation) a maintained hyperpolarization. Taken together with the observations that low concentrations of caesium potently block I_h, the sag, and the overshoot, these data indicate that I_h activation and deactivation underlie the sag and overshoot phenomena described by Mason & Larkman (1990) in at least a portion of their *thick* layer 5 cells. This finding is consistent with descriptions of the actions of I_h in other systems (Fain *et al.* 1978; Atwell & Wilson, 1980; Mayer & Westbrook, 1983; Spain *et al.* 1987) in which I_h can decrease the voltage change caused by hyperpolarizing inputs and lead to an overshoot of the rest potential following current injections. I_h in SCP neurons would be expected to modulate, in a similar fashion, responses to sustained hyperpolarizing *synaptic* inputs, such as $GABA_B$-mediated IPSPs (Newberry & Nicoll, 1985; Connors, Malenka & Silva, 1988). I_h activation during $GABA_B$-mediated potassium conductance increases would be expected to attenuate the degree of cellular hyperpolarization. Following the IPSP, the slow deactivation of I_h could cause a transient depolarizing overshoot of the resting membrane potential leading to the firing of one or more action potentials. Anatomical evidence suggests that layer 5 cells in general (C. McDonald & A. Burkhalter, personal communication) and SCP cells in particular (Gabbott, Martin & Whitteridge, 1988) receive dense GABAergic inputs. I_h in SCP neurons could thus contribute to the generation of stereotyped *rebound* firing patterns (Crunelli & Leresche, 1991) following synaptic inhibition. Because this work was performed on identified neurons, such hypotheses can be tested by examining not only the responses of SCP neurons to inhibitory neurotransmitters *in vitro*, but also the anatomical and physiological details of inhibitory synaptic contacts on these cells in intact preparations.

We thank Mr John Doyle, Mr Joe Doyle, and Dr Kelleen Giffin for their excellent technical assistance in the preparation and maintenance of cortical cultures. We are also greatly indebted to Dr Andreas Burkhalter for his enthusiastic support of this project, his assistance with cell labelling and identification, and for numerous helpful discussions. We also thank Dr Bob Wilkinson for his invaluable assistance in the design of the switch clamp, and for numerous helpful discussions. Finally, we thank Drs Jim Huettner, Chris Lingle and Joe-Henry Steinbach for their critical reviews of this manuscript. This work was supported by the National Science Foundation (BNS-8809823) and the National Institutes of Health (T32-GM07205, T32-GM07200).

REFERENCES

ANGSTADT, J. D. & CALABRESE, R. L. (1989). A hyperpolarization-activated inward current in heart interneurons of the medicinal leech. *Journal of Neuroscience* **9**, 2846–2857.

ATWELL, D. & WILSON, M. (1980). Behaviour of the rod network in the tiger salamander retina mediated by membrane properties of individual rods. *Journal of Physiology* **309**, 287–315.

BADER, C. R., MACLEISH, P. R. & SCHWARTZ, E. A. (1979). A voltage-clamp study of the light response in solitary rods of the tiger salamander. *Journal of Physiology* **296**, 1–26.

BROWN, H. F., DIFRANCESCO, D. & NOBLE, S. J. (1979). How does adrenaline accelerate the heart? *Nature* **280**, 235–236.

CONNORS, B. W. & GUTNICK, M. J. (1990). Intrinsic firing patterns in diverse neocortical neurons. *Trends in Neuroscience* **13**, 99–104.

CONNORS, B. W., MALENKA, R. C. & SILVA, L. R. (1988). Two inhibitory postsynaptic potentials, and $GABA_A$ and $GABA_B$ receptor-mediated responses in neocortex of the rat and cat. *Journal of Physiology* **406**, 443–468.

CRUNELLI, V. & LERESCHE, N. (1991). A role for $GABA_B$ in excitation and inhibition of thalamocortical cells. *Trends in Neuroscience* **14**, 16–21.

DIFRANCESCO, D. (1981). A study of the ionic nature of the pace-maker current in calf Purkinje fibres. *Journal of Physiology* **314**, 377–393.

DIFRANCESCO, D. (1982). Block and activation of the pace-maker channel in calf Purkinje fibres: effects of potassium, caesium and rubidium. *Journal of Physiology* **329**, 485–507.

EDMAN, Å., GESTRELIUS, S. & GRAMPP, W. (1987). Current activation by membrane hyperpolarization in the slowly adapting lobster stretch receptor neurone. *Journal of Physiology* **384**, 671–690.

EDMAN, Å. & GRAMPP, W. (1989). Ion permeation through hyperpolarization-activated membrane channels (Q-channels) in the lobster stretch receptor neurone. *Pflügers Archiv* **413**, 249–255.

FAIN, G. L., QUANDT, F. N., BASTIAN, B. L. & GERSCHENFELD, H. M. (1978). Contribution of a caesium-sensitive conductance increase to the rod photoresponse. *Nature* **272**, 467–469.

FUTAMACHI, K. J., MUTANI, R. & PRINCE, D. A. (1974). Potassium activity in rabbit cortex. *Brain Research* **75**, 5–25.

GABBOTT, P. L. A., MARTIN, K. A. C. & WHITTERIDGE, D. (1988). Evidence for the connections between a clutch cell and a corticotectal neuron in area 17 of the cat visual cortex. *Proceedings of the Royal Society of London* B **233**, 385–391.

GIFFIN, K., SOLOMON, J. S., BURKHALTER, A. & NERBONNE, J. M. (1991). Differential expression of voltage-gated calcium channels in identified visual cortical neurons. *Neuron* **6**, 321–332.

GOLDMAN, D. E. (1943). Potential, impedance, and rectification in membranes. *Journal of General Physiology* **27**, 37–60.

HAGIWARA, N. & IRISAWA, H. (1989). Modulation by intracellular Ca^{2+} of the hyperpolarization-activated inward current in rabbit single sino-atrial node cells. *Journal of Physiology* **409**, 121–141.

HAGIWARA, S., MIYAZAKI, S. & ROSENTHAL, N. P. (1976). Potassium current and the effect of caesium on this current during anomalous rectification of the egg cell membrane of a starfish. *Journal of General Physiology* **67**, 621–638.

HALLMAN, E. R., SCHOFIELD, B. R. & LIN, C.-S. (1988). Dendritic morphology and axon collaterals of corticotectal, corticopontine, and callosal neurons in layer V of primary visual cortex of the hooded rat. *Journal of Comparative Neurology* **272**, 149–160.

HAMILL, O. P., MARTY, A., NEHER, E., SAKMANN, B. & SIGWORTH, F. J. (1981). Improved patch-clamp techniques for high resolution current recording from cells and cell-free membrane patches. *Pflügers Archiv* **391**, 85–100.

HESTRIN, S. (1987). The properties and function of inward rectification in rod photoreceptors of the tiger salamander. *Journal of Physiology* **390**, 319–333.

HODGKIN, A. L. & KATZ, B. (1949). The effect of sodium ions on the electrical activity of the giant axon of the squid. *Journal of Physiology* **108**, 37–77.

HORN, R. & MARTY, A. (1988). Muscarinic activation of ionic currents measured by a new whole-cell recording method. *Journal of General Physiology* **92**, 145–159.

HOTSON, J. R., SYPERT, G. W. & WARD, A. A. JR (1973). Extracellular potassium concentration changes during propagated seizures in neocortex. *Experimental Neurology* **38**, 20–26.

HUETTNER, J. E. & BAUGHMAN, R. W. (1986). Primary culture of identified neurons from the visual cortex of postnatal rats. *Journal of Neuroscience* **6**, 3044–3060.

KATZ, L. C., BURKHALTER, A. & DREYER, W. J. (1984). Fluorescent latex microspheres as a retrograde neuronal marker for *in vivo* and *in vitro* studies of visual cortex. *Nature* **310**, 498–500.

LARKMAN, A. & MASON, A. (1990). Correlations between morphology and electrophysiology of pyramidal neurons in slices of rat visual cortex. I. Establishment of cell classes. *Journal of Neuroscience* **10**, 1407–1414.

MCCORMICK, D. A. & PAPE, H.-C. (1990). Properties of a hyperpolarization-activated cation current and its role in rhythmic oscillation in thalamic relay neurones. *Journal of Physiology* **431**, 291–318.

MASON, A. & LARKMAN, A. (1990). Correlations between morphology and electrophysiology of pyramidal neurons in slices of rat visual cortex. II. Electrophysiology. *Journal of Neuroscience* **10**, 1415–1428.

MAYER, M. L. & WESTBROOK, G. L. (1983). A voltage-clamp analysis of inward (anomalous) rectification in mouse spinal sensory ganglion neurones. *Journal of Physiology* **340**, 19–45.

NEWBERRY, N. R. & NICOLL, R. A. (1985). Comparison of the action of baclofen with γ-aminobutyric acid on rat hippocampal pyramidal cells *in vitro*. *Journal of Physiology* **360**, 161–185.

OHNO, M., OBRENOVITCH, T. P., HÅRTELL, N., BARRATT, S., BACHELARD, H. S. & SYMON, L. (1989). Simultaneous recording of tissue P_{CO_2}, interstitial pH and potassium activity in the rat cerebral cortex during anoxia and the subsequent recovery period. *Neurological Research* **11**, 153–159.

RAFF, M. C., FIELDS, K. L., HAKOMORI, S., MIRSKY, R., PRUSS, R. M. & WINTER, J. (1979). Cell type-specific markers for distinguishing and studying neurons and the major classes of glial cells in culture. *Brain Research* **174**, 283–308.

SCHIELKE, G. P., MOISES, H. C. & BETZ, A. L. (1991). Blood to brain sodium transport and interstitial fluid potassium concentration during early focal ischemia in the rat. *Journal of Cerebral Blood Flow and Metabolism* **11**, 466–471.

SCHOFIELD, B. R., HALLMAN, L. E. & LIN, C.-S. (1987). Morphology of corticotectal cells in the primary visual cortex of hooded rats. *Journal of Comparative Neurology* **261**, 85–97.

SILVA, L. R., AMITAI, Y. & CONNORS, B. W. (1991). Intrinsic oscillations of neocortex generated by layer 5 pyramidal neurons. *Science* **251**, 432–435.

SPAIN, W. J., SCHWINDT, P. C. & CRILL, W. E. (1987). Anomalous rectification in neurons from cat sensorimotor cortex *in vitro*. *Journal of Neurophysiology* **57**, 1555–1576.

THONG, I. G. & DREHER, H. (1986). The development of the corticotectal pathway in the albino rat. *Developmental Brain Research* **25**, 227–238.

VYSKOČIL, F., KŘÍŽ, N. & BUREŠ, J. (1972). Potassium-selective microelectrodes used for measuring the extracellular brain potassium during spreading depression and anoxic depolarization in rats. *Brain Research* **39**, 255–259.

YANAGIHARA, K. & IRISAWA, H. (1980). Inward current activated during hyperpolarization in the rabbit sinoatrial node cell. *Pflügers Archiv* **385**, 11–19.